metals

MDPI

Article

Study on Reduction Mechanism of Iron Oxide by Industrial Lignin

Dongwen Xiang [1,*], Qiang Zhang [1], Guoqing Wu [2], Yajie Wang [1], Dong Li [1], Qinghua Zhang [1] and Huaxin Hu [1]

[1] School of Materials Science and Engineering, Linyi University, Linyi 276003, China; zhangqiang@lyu.edu.cn (Q.Z.); wangyajie@lyu.edu.cn (Y.W.); lidong489@lyu.edu.cn (D.L.); qhzhang@lyu.edu.cn (Q.Z.); huhuaxin@lyu.edu.cn (H.H.)

[2] School of Materials Science and Engineering, Beihang University, Beijing 100191, China; guoqingwu@buaa.edu.cn

* Correspondence: xiangdongwen1@163.com

Abstract: To effectively utilize industrial lignin, a large amount of waste produced by the pulp and paper industry, this paper primarily explores its potential as a substitute for coal-based reducing agents in the reduction of iron oxides. The weight change, phase change, and activation energy change during the reduction of iron oxide by industrial lignin were characterized using detection methods such as TG-DTG-DSC, XRD, and SEM. The results show that the maximum weight loss rate of industrial lignin reducing iron oxide is (4.52%·min^{-1}) > Lu'an anthracite (2.01%·min^{-1}) > Shenmu bituminous coal (1.57%·min^{-1}). The activation energy variation range during the reduction of Fe_2O_3 by industrial lignin, calculated using the Flynn–Wall–Ozawa (FWO) method, is 241.91~463.51 kJ·mol^{-1}, and the activation energy first decreased, then increased, then decreased slightly with the increase of conversion fraction. There is a coupling effect in the reduction of Fe_2O_3 by industrial lignin.

Keywords: industrial lignin (IL); ferric oxide; reduction; activation energy

Citation: Xiang, D.; Zhang, Q.; Wu, G.; Wang, Y.; Li, D.; Zhang, Q.; Hu, H. Study on Reduction Mechanism of Iron Oxide by Industrial Lignin. *Metals* **2024**, *14*, 1467. https://doi.org/10.3390/met14121467

Academic Editors: Srecko Stopic and Petros E. Tsakiridis

Received: 6 October 2024
Revised: 9 December 2024
Accepted: 19 December 2024
Published: 23 December 2024

1. Introduction

About 20 million tons of industrial lignin is contained in the waste liquid produced by China's pulp and paper industry every year, and more than 98% of the industrial lignin is still directly discharged into rivers as waste liquid or burned after concentration. Less than 2% of the total industrial lignin is recycled and made into low value-added products, which not only wastes resources but also pollutes the environment [1–4]. The reuse of industrial lignin resources is one of the urgent problems to be solved in the pulp and paper industry.

Lignin is used in a variety of ways and can be used directly as a chemical. However, it is necessary to adjust its structure to enhance its functionality, such as increasing the reactivity of hydroxyl groups or changing the properties of chemical reaction sites, so as to synthesize more efficient and reactive macromonomers [5]. The chemical modification reactions on the surface of lignin include esterification, etherification, benzene alcoholization, silylation, oxidation-reduction, and reactions with isocyanates [6], mainly including alkylation/dealkylation, hydroxyalkylation, amination, and nitration, aiming to control the amphiphilic and solubility of lignin and increase its applicability as a catalytic reaction group [7]. In the field of polymer science, the direct application of lignin includes the development of mixtures and biocomposites that help replace traditional polyolefins without affecting the mechanical strength of composites [8]. In biocomposites, lignin can be used as a phase solvent for a variety of polymers [9], a dye remover [10], a fire-resistant composite material [11], a manufacturing film [12], and a polyelectrolyte film [13]. In addition, due to the reduction functional groups contained in the lignin structure, researchers have also used its reduction properties to prepare metal nanoparticles such as palladium and silver [14].

Lignin is also used to produce precursor materials for carbon-based materials such as activated carbon, carbon catalyst, carbon fiber, and carbon electrode [15].

Another way to utilize lignin is to obtain small molecular products by pyrolysis, oxidative depolymerization, reductive depolymerization, biological depolymerization, etc., which can be used as raw materials for the preparation of other chemicals [16]. The main products of lignin pyrolysis are bio-oil, combustible gas, and char [17–20]. Other researchers have found that adding a catalyst can improve the depolymerization efficiency of lignin, product yield, and selectivity, and reduce the occurrence of polymerization reaction [21–23]. Oxidative depolymerization of lignin refers to the depolymerization of lignin under the action of low temperature (30~250 °C) and oxidants (hydrogen peroxide, nitrobenzene, metal oxides, oxygen, and Fenton reagents), which can produce small molecule carboxylic acids (oxalic acid and acetic acid) and a variety of aromatic chemicals, such as aromatic aldehydes (vanillin and syringaldehyde) and benzene carboxylic acids (vanillin and syringic acid), including processes of electrocatalytic oxidation, photocatalytic oxidation, heterogeneous catalytic oxidation, and ionic liquid catalytic oxidation [24–27]. The reductive depolymerization of lignin refers to the pyrolysis of lignin under the action of reducing agent (H_2 or hydrogen donor solvent). At present, a variety of reaction paths and mechanisms have been proposed for the reduction and depolymerization of lignin, mainly including the hydrogenolysis of ether linkages and the removal of hydroxyl groups [28–31]. Biological depolymerization of lignin refers to the process of depolymerization of lignin to simple aromatic compounds under relatively mild conditions with the assistance of enzymes (laccase, lignin peroxidase, aryl alcohol oxidase, β-etherase, etc.), bacteria (such as white-rot fungi), or fungi (such as *Rhodococcus* opaque) [32–34].

At present, the yield and selectivity of lignin depolymerization products have not been high. The oxidation process leads to the destruction of the aromatic structure and the waste of aromatic resources [35]. The monomer yield obtained in the hydrogenation process is about 10~50% [36], which limits the further transformation and application of lignin. There are few reports on the reduction of iron oxide by industrial lignin. This paper mainly studies the kinetics and phase change of industrial lignin in the process of reducing iron oxide, and reveals its reaction mechanism and phase change law, in order to use the industrial lignin produced by the pulp and paper industry in the iron making industry. This can not only improve the energy structure of iron making production and reduce CO_2 emissions, but also consume a large amount of carbon-containing waste from the pulp and paper industry, reduce the impact of disorderly combustion on the environment, and improve the utilization efficiency of waste, which has obvious environmental protection advantages and social benefits.

2. Materials and Methods

2.1. Experimental Materials

The reducing agents used in the experiment included IL, Lu'an anthracite (LA), and Shenmu bituminous coal (SM). LA and SM were provided by an iron and steel company (Anyang, China), while IL was provided by Huawei Youbang Chemical Co., Ltd. (Tumen, China). The proximate analysis and elemental analysis methods of three reducing agents are shown in Reference [37], and the results are shown in Table 1. The hematite powder was provided by Sinopharm Chemical Reagent Beijing Co., Ltd. (Beijing, China), containing Fe_2O_3 of more than 99.9%.

Table 1. Proximate analysis and elemental analysis of pulverized coal and IL (mass, %).

Samples	Proximate Analysis (ad.)				Elemental Analysis (ad.)				
	Fixed Carbon	Ash	Volatile	Moisture	C	H	O	N	S
IL	26.35	8.31	60.44	4.89	59.56	6.82	29.67	0.20	1.82
LA	75.90	10.01	13.38	0.71	82.00	3.41	8.50	1.79	0.20
SM	62.41	7.46	28.28	1.85	75.90	4.14	16.50	1.38	0.63

ad.: air-dried basis.

2.2. Apparatus and Experimental Procedures

The weight loss behavior of three reducing agents mixed with iron oxide reagent was studied on a thermogravimetric analyzer (STA409CD, NETZSCH Group, Hanau, Germany) under the nitrogen atmosphere. The mixing ratio of reducing agent and iron oxide is determined according to the molar ratio of carbon to oxygen of 1.0, that is n_c:n_o = 1.0, wherein n_c is the mole fraction of total carbon in the reducing agent and n_o is the mole fraction of oxygen in iron oxide. In this work, about 10 mg of the mixed sample was placed in an alumina crucible and heated from ambient temperature up to 1100 °C at heating rates of 5, 10, and 15 °C·min^{-1} under an N_2 flow at 30 mL·min^{-1}. The production of metalized pellets is mainly based on the grate–rotary kiln process, which has a very fast heating rate [38,39]. The closed crucible used in this experiment was an alumina crucible with a capacity of 70 µL. A separate blank run was conducted using an empty pan under identical conditions and these data were used for baseline correction during the evaluation of the sample thermal gravimetric analysis (TGA) profile. In order to analyze the reduction process of the mixed sample, we obtained the weight–temperature data when the reducing agent was heated from 30 °C to 1100 °C. The test scheme is shown in Table 2.

Table 2. Experimental design on the reduction of Fe_2O_3 by different reducing agents.

Number	Samples	n_c/n_o	Heating Rate (°C·min^{-1})
S1	LA	---	10
S2	SM	---	10
S3	IL	---	10
S4	LA + Fe_2O_3	1.0	5, 10, 15
S5	SM + Fe_2O_3	1.0	5, 10, 15
S6	IL + Fe_2O_3	1.0	5, 10, 15

The phase and morphology of the samples were analyzed by D8ADVANCE X-ray diffractometer (XRD, Bruker, Bremen, Germany) and JSM-6510LV scanning electron microscope (SEM, Electronics Company, Tokyo, Japan).

2.3. Kinetic Equation

Due to the fact that the reduction of Fe_2O_3 by IL involves both biomass pyrolysis and the reduction of Fe_2O_3 by pyrolysis products, it cannot be described by a reasonable mechanism function. However, the iso-conversion method can obtain a more reliable reaction activation energy without involving the kinetic mode function, thus avoiding the adverse effects of the model on the experimental results. Therefore, two iso-conversion methods, Flynn–Wall–Ozawa (FWO) and Kissinger–Akah–Sunose (KAS), were used to analyze the reduction process [40–44].

The general chemical reaction kinetic Equations are (1) and (2).

$$\frac{d\alpha}{dt} = \beta\frac{d\alpha}{dT} = k(T)f(\alpha) = A\exp(-\frac{E}{RT})f(\alpha) \quad (1)$$

$$G(\alpha) = \int_0^\alpha \frac{1}{f(\alpha)}\mathrm{d}\alpha = \int_0^t A\exp(-\frac{E}{RT})\mathrm{d}t \quad (2)$$

Bring $\beta = dT/dt$ into Formula (2) to get Formula (3):

$$G(\alpha) = \int_0^t A\exp\left(-\frac{E}{RT}\right)dt = \frac{A}{\beta}\int_{T_0}^{T}\exp\left(-\frac{E}{RT}\right)dT \approx \frac{A}{\beta}\int_0^T \exp\left(-\frac{E}{RT}\right)dT = \frac{AE}{\beta R}\int_{\mu_T}^{\infty}\frac{\exp(-\mu)}{\mu^2}dT \quad (3)$$

Take the logarithm of both sides of Formula (3) to obtain Formula (4):

$$\ln\left[\frac{\beta}{T^2}\right] = \ln\left[\frac{AR}{G(\alpha)E}\right] - \frac{E}{RT} \quad (4)$$

Using the Doyle method to approximate the temperature integral of equation $\int_{T_0}^{T}\exp\left(-\frac{E}{RT}\right)dT$, Formula (5) is obtained:

$$\ln\beta = \ln\left(\frac{AE}{RG(\alpha)}\right) - 5.331 - 1.052\frac{E}{RT} \quad (5)$$

where β is the heating rate, K·min^{-1}; R is the gas constant, 8.314 J·mol^{-1}·k^{-1}; $k(T)$ is the rate constant at temperature T; $f(\alpha)$ is the function of conversion rate α, representing the differential formula of kinetic mechanism function; A is the pre-exponential factor, min^{-1}; E is the activation energy, J·mol^{-1}; $G(\alpha)$ is the integral formula of the kinetic mechanism function; μ_T is the corresponding μ value at temperature T; and $\mu = E/(RT)$.

Formula (4) is a general formula for the KAS method. Linear regression is performed on T^{-1} using $\ln(\beta/T^2)$, and the corresponding activation energy value at the corresponding conversion rate is determined based on the slope of the fitted line ($-E/R$). Formula (5) is a general formula for the FWO method. Linear regression is performed on T^{-1} using $\ln\beta$, and the corresponding activation energy value at the corresponding conversion rate is determined based on the slope of the fitted line ($-1.052E/R$).

In this study, ten different conversion rates (α = 0.1, 0.2, 0.3, 0.4, 0.5, 0.6, 0.7, 0.8, 0.9 and 0.95) were selected, and the activation energy was obtained by FWO and KAS methods to determine the appropriate model to describe the reduction of Fe_2O_3 by IL.

3. Results and Discussions

3.1. Comparison of Reducing Agent Pyrolysis and Its Reduction of Fe_2O_3

The pyrolysis process of reducing agent alone, and the reduction process of Fe_2O_3 mixed with different reducing agents (n_c/n_o = 1, heating rate is 10 °C·min^{-1}) are shown in Figure 1. TG curve and DTG curve in the figure are the weight loss process and weight loss rate of the sample, respectively. The purpose of setting pulverized coal in this paper is to compare it with the results of lignin reducing iron oxide.

It can be seen from the figure that: (1) The DTG curve of Fe_2O_3 reduction will appear as an obvious peak in the high temperature region, while the DTG curve of the reductant pyrolysis alone does not, which indicates that the reduction of iron oxide occurs in the high temperature stage. (2) The maximum reaction rates of reducing Fe_2O_3 by the three reducing agents are in descending order: IL (4.53%/min) > LA (2.01%/min) > SM (1.57%/min). (3) The temperature corresponding to the maximum reduction rate of Fe_2O_3 by IL is lower than that of two kinds of pulverized coal. (4) When the temperature reaches 900 °C, the TG curve of IL reducing Fe_2O_3 no longer changes, which indicates that the reduction reaction has been basically completed. However, in the process of reducing Fe_2O_3 by two pulverized coals, the TG curve still has a downward trend when the temperature is 1100 °C, which indicates that Fe_2O_3 has not been completely reduced at this time.

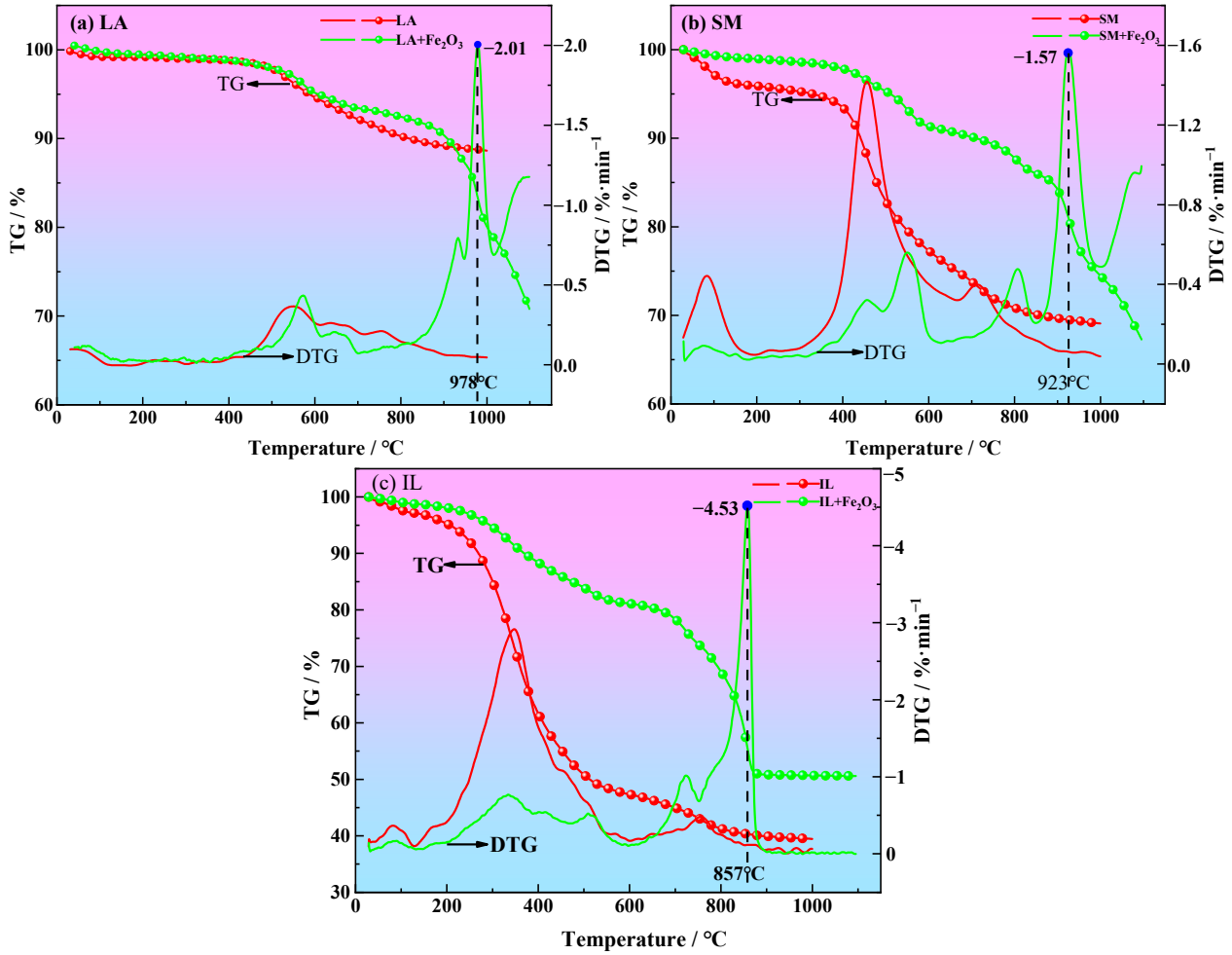

Figure 1. Thermogravimetric curve of reducing agent pyrolysis and its reduction of Fe_2O_3 at heating rate of 10 °C·min^{-1}.

3.2. Phase Transformation During Reduction of Fe_2O_3

Under the condition of a heating rate of 10 °C·min^{-1}, the phase composition at different temperatures during the reduction of Fe_2O_3 by three reducing agents was studied. The results are shown in Figure 2.

When the reduction temperature was 600 °C, Fe_2O_3 still existed in the sample mixed with pulverized coal and Fe_2O_3, while Fe_2O_3 was completely reduced to Fe_3O_4 in the sample mixed with IL and Fe_2O_3, as shown in Figure 2a. When the temperature reached 700 °C, Fe_2O_3 in all three mixed samples was completely reduced to Fe_3O_4, and FeO appeared in the mixed sample of IL and Fe_2O_3, while it had not yet appeared in the mixed sample of pulverized coal. When the reduction temperature was 800 °C, FeO appeared in the three mixed samples, but a small amount of Fe appeared in the mixed samples of IL and Fe_2O_3. When the reduction temperature reached 900 °C, the mixed sample of pulverized coal and Fe_2O_3 completed the transformation of Fe_3O_4→FeO, while the mixed sample of IL and Fe_2O_3 completed the transformation of FeO→Fe. When the temperature reached 1000 °C, Fe began to appear in the mixed sample of pulverized coal and Fe_2O_3. At 1100 °C, the transformation of FeO→Fe was completed in the mixed sample of pulverized coal and Fe_2O_3. From the above analysis, it can be concluded that the reduction of Fe_2O_3 by IL is easier than that by pulverized coal.

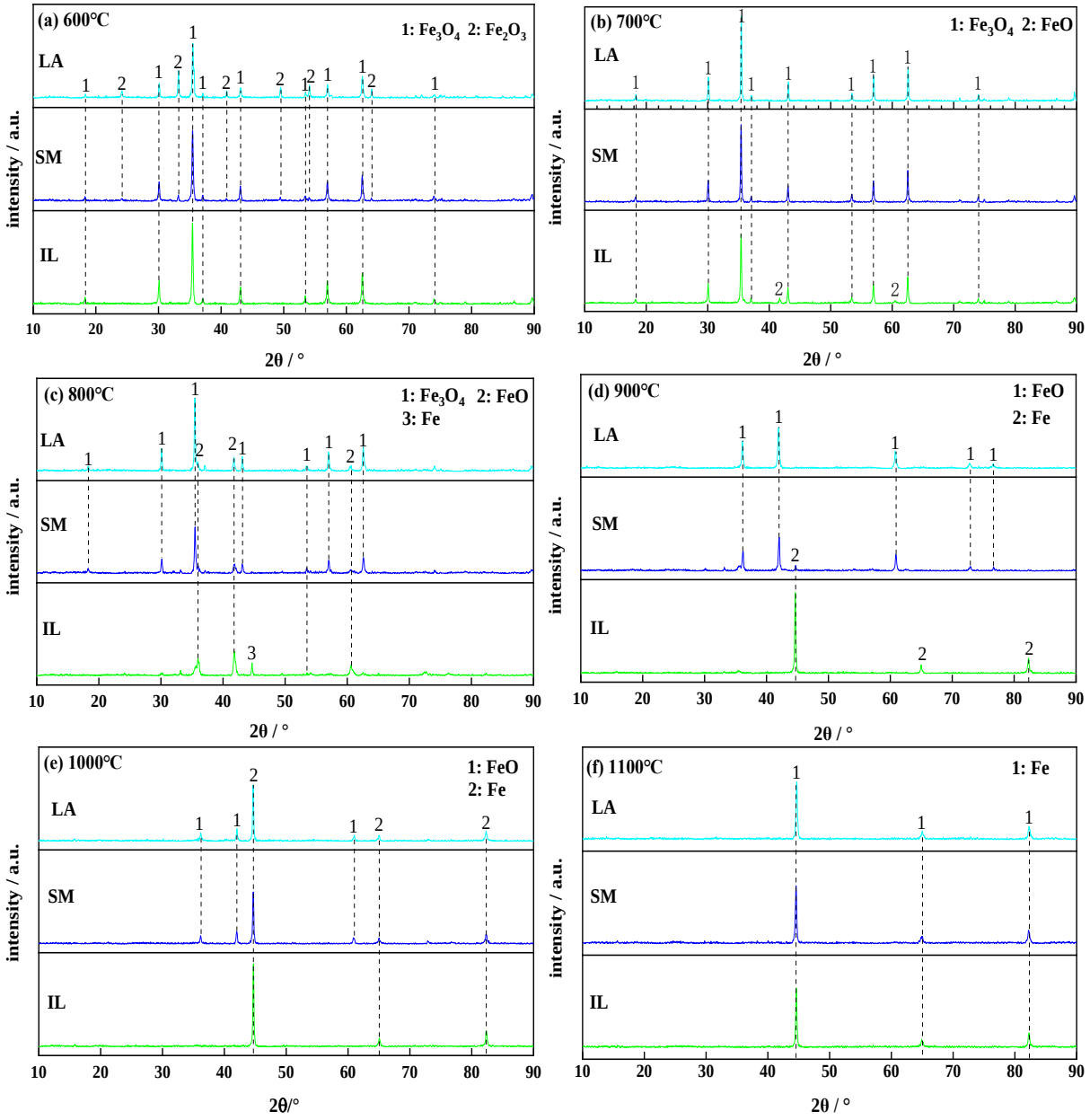

Figure 2. Phase composition of mixed samples of different reductants and Fe_2O_3 under conditions of n_c/n_o = 1 and heating rate of 10 °C·min^{-1}.

In addition, the surface morphology of the IL and Fe_2O_3 mixed samples heated to different temperatures at a heating rate of 10 °C/min was observed, and the results are shown in Figure 3.

When the reduction temperature was 600 °C, the surface of the sample began to gather iron-containing substances; iron whiskers appeared until the temperature rose to 900 °C, which is consistent with the XRD test results in Figure 2d. When the reduction temperature was 1100 °C, the iron whiskers became coarse and full. It can be seen from Figure 3 that the resulting particle size slightly decreased with the increase of temperature. Since the amount of reducing agent added in the mixed sample is calculated according to the total carbon, not only the pyrolysis product of the reducing agent will have a reduction effect on the iron oxide, but also the carbon in the reducing agent will have a reduction effect on the iron oxide. Combined with the SEM-EDS analysis in Figure 3d–f, it can be seen that the carbon in the mixed sample was excess. Therefore, the mechanism of inhibiting the growth of iron whiskers is that the carbon coated on the surface of mineral powder can replace the

formation of metal Fe core and block the contact between new pig iron, so as to inhibit the growth of iron whiskers [45,46]. Finally, the size of the iron-joined crystal was reduced.

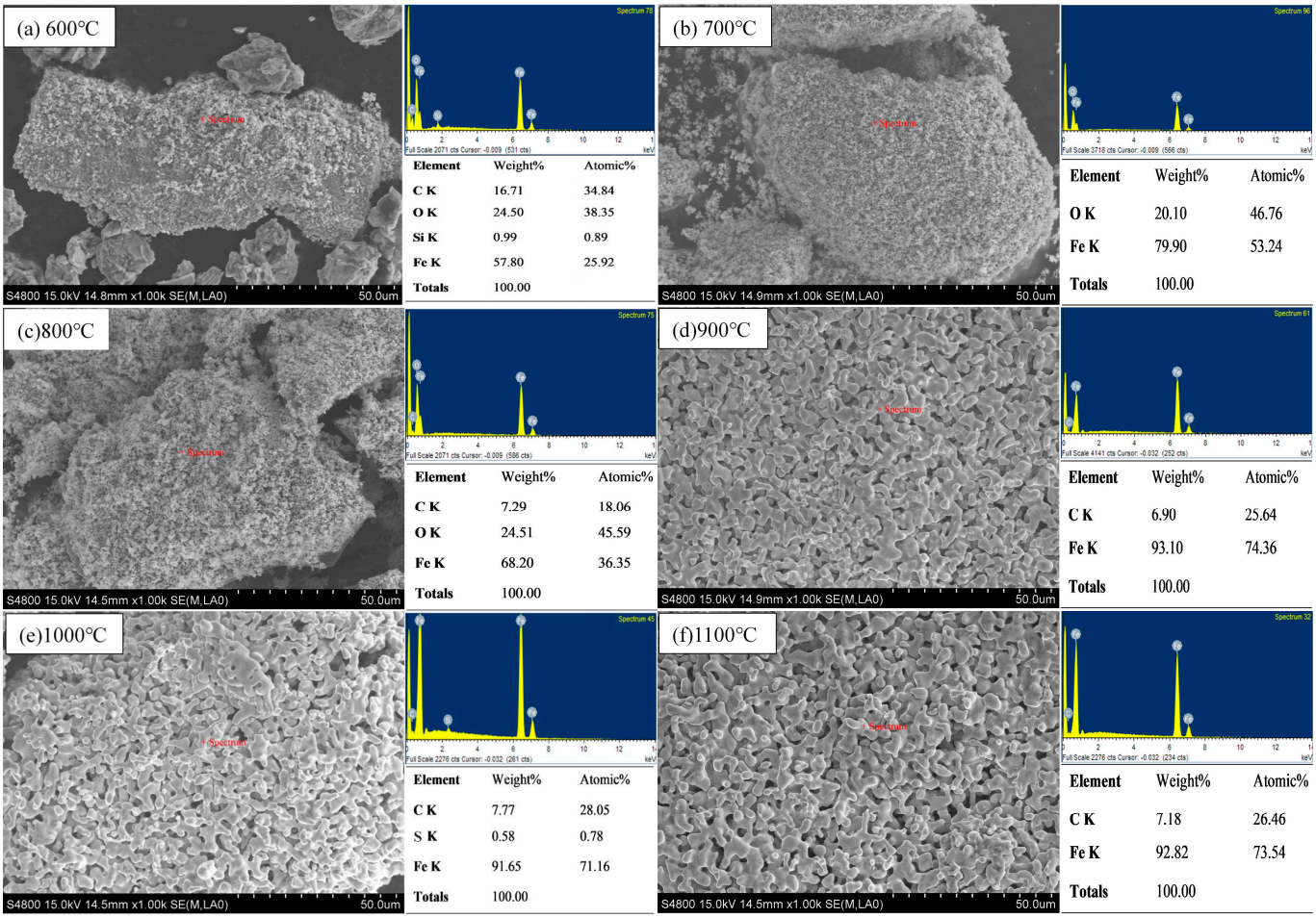

Figure 3. SEM-EDS diagram of IL + Fe_2O_3 mixed sample after reduction at heating rate of 10 °C·min^{-1}.

3.3. Effect of Heating Rate on the Reduction of Fe_2O_3

The effect of heating rate on Fe_2O_3 reduction is shown in Figure 4. It can be seen that with the increase of heating rate, the weight loss curve shifts from low temperature to high temperature zone. This is because a higher heating rate affects the heat transfer temperature difference and temperature gradient between the test point and the sample, as well as between the outer and inner samples, leading to an aggravation of thermal hysteresis phenomenon. In addition, it is found that the heating rate also has a certain influence on the maximum weight loss rate, that is, the maximum weight loss rate will decrease with the increase of the heating rate. For example, when the heating rate was 5 °C·min^{-1}, the maximum weight loss rate of IL reducing Fe_2O_3 was 0.46%/°C. When the heating rate was 10 °C·min^{-1}, the maximum weight loss rate decreased to 0.16%/°C. When the heating rate was continuously increased to 15 °C·min^{-1}, the maximum weight loss rate was reduced to 0.14%/°C.

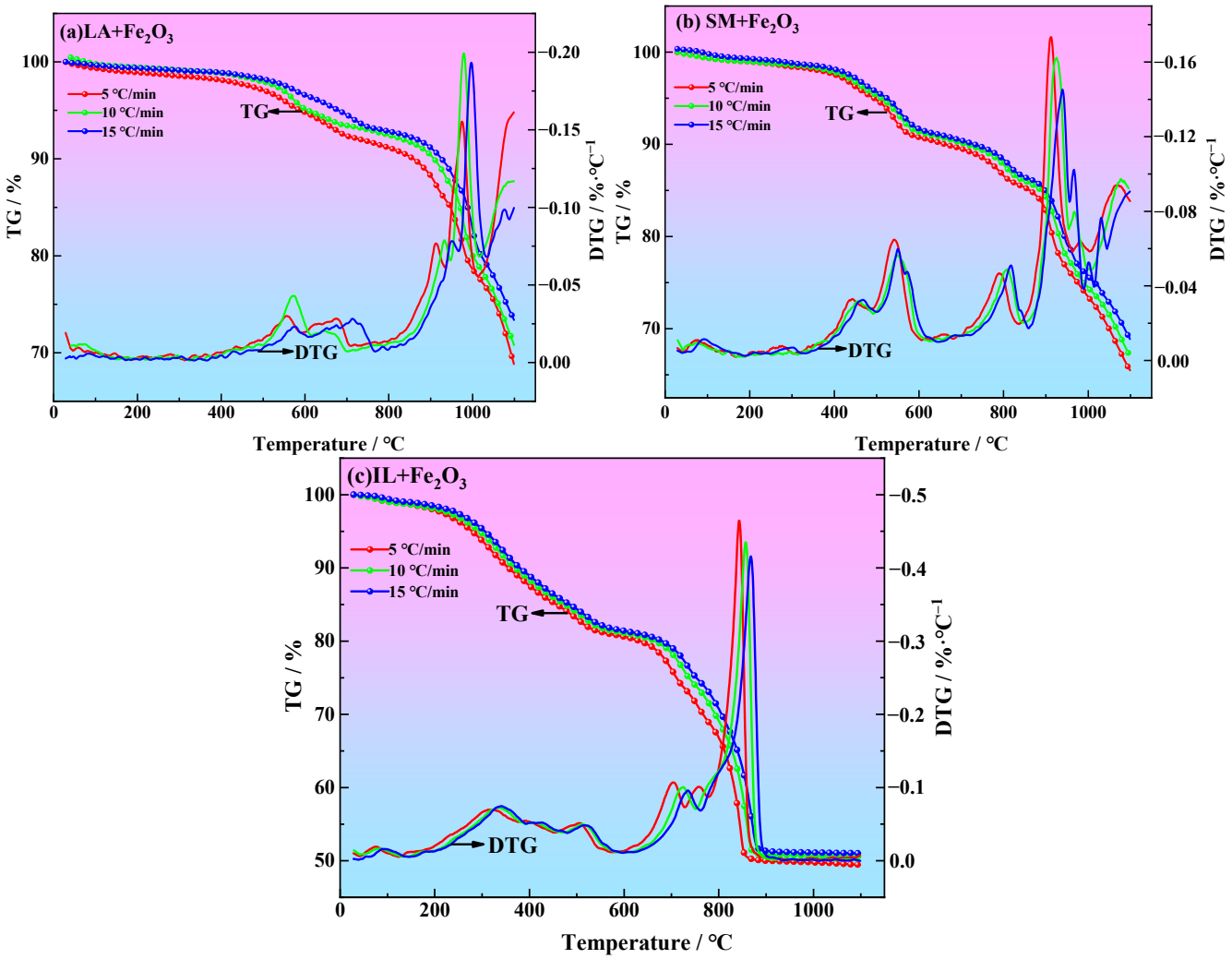

Figure 4. TG-DTG curve of Fe_2O_3 reduction process under different heating rates. (**a**) LA + Fe_2O_3; (**b**) SM + Fe_2O_3; (**c**) IL + Fe_2O_3.

From the above analysis, it can be found that an excessively high heating rate has an adverse effect on the reduction of Fe_2O_3. This is related to the heat and mass transfer inside and outside the IL particles, as well as the specific surface area of the product char. When the heating rate is low, the IL particles are uniformly heated from the inside out, and the pyrolysis is rapid, generating more reducing substances containing C and H, which is conducive to the reduction reaction. However, if the heating rate is too high, the pyrolysis reaction time of pulverized coal or IL will be shortened, the pyrolysis products will be reduced, and the volatile components of the reducing agent will be devolatilization at a higher temperature, mostly in the form of tar. The tar condenses inside and on the surface of char particles, reducing and blocking some of the char pores generated by the devolatilization, resulting in a decrease in the reaction area between char and Fe_2O_3. In addition, the high heating rate increases the residence time of char at high temperature, which in turn causes the small pores in the char to sinter and fuse, and the specific surface area becomes smaller. Finally, the reduction reaction is hindered. Therefore, on the basis of ensuring both sufficient reduction and reduction efficiency, the optimal heating rate is suggested to be 10 °C·min^{-1}.

3.4. Kinetic Study on the Reduction of Fe_2O_3

In this study, the isoconversional method was used to determine the change of activation energy with the conversion rate, so as to reveal the essence that seemingly simple reactions are actually complex reactions [47], the kinetic analysis of IL + Fe_2O_3 sample under the condition of n_c/n_o = 1.0 was analyzed. The obtained activation energy can be compared with the activation energy during the reduction of iron oxide by pulverized coal or other biomass, indicating the potential of industrial lignin for the ironmaking industry. The TG-DTG-DSC curve of the sample at a heating rate of 10 °C·min^{-1} is shown in Figure 5. When the temperature exceeds 600 °C, the weight loss rate of the sample begins to increase, and the DSC curve begins to show an endothermic peak. Combined with Figure 2a, this indicates that Fe_2O_3 has begun to be reduced to Fe_3O_4.

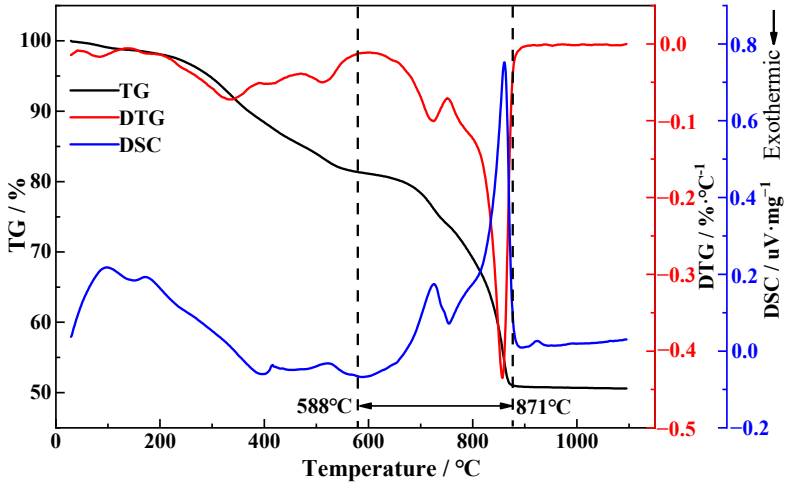

Figure 5. TG-DTG-DSC curve of reduction of iron oxide by IL at heating rate of 10 °C·min^{-1}.

The TG and DSC curves in Figure 5 stabilized around 900 °C, and combined with Figure 3, this indicates that Fe_2O_3 has been completely reduced to Fe when the temperature reaches 900 °C. Therefore, under the condition of a heating rate of 10 °C·min^{-1}, the reduction temperature range of Fe_2O_3→Fe_3O_4→Fe in the mixed sample of IL and Fe_2O_3 can be determined to be 588~871 °C.

Based on the above analysis, the temperature range division of Fe_2O_3 reduction in IL and Fe_2O_3 mixed samples under different heating rates is shown in Table 3.

Table 3. Division of reduction temperature interval.

Samples	Heating Rate (°C·min^{-1})	Reduction Temperature Range (°C)
IL + Fe_2O_3	5	578~858
	10	588~871
	15	599~883

The kinetic fitting curves of the reduction of Fe_2O_3 by IL using FWO and KAS methods (reduction temperature range in Table 3) are shown in Figure 6 and Figure 7, respectively. The relevant kinetic parameters obtained by the above two methods are shown in Table 4 and Table 5, respectively.

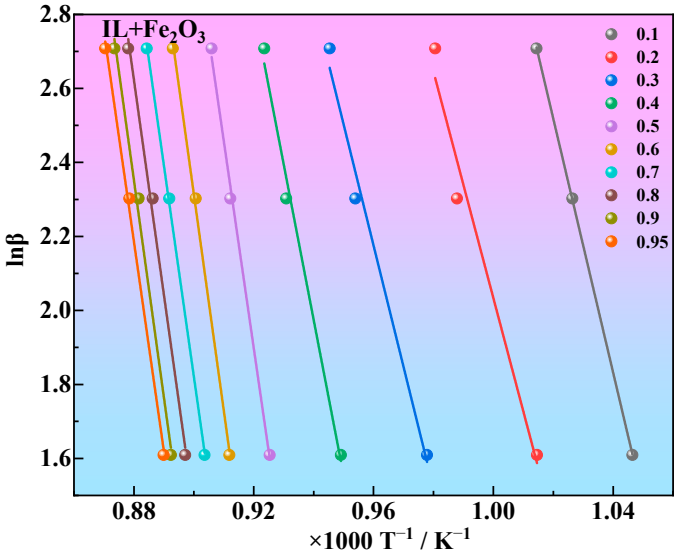

Figure 6. Linear fitting relationship between $\ln\beta$ and $1/T$ under different conversion rates calculated by FWO method.

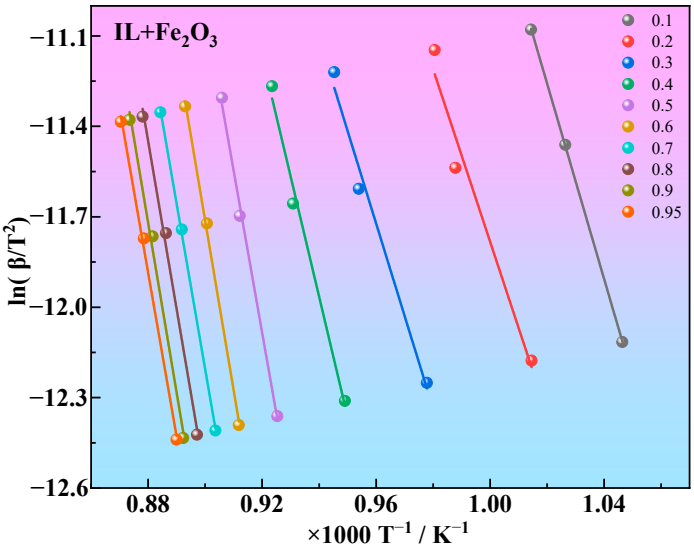

Figure 7. Linear fitting relationship between $\ln(\beta/T^2)$ and $1/T$ under different conversion rates calculated by KAS method.

According to the analysis of Figures 6 and 7, as well as Tables 4 and 5, it can be seen that the FWO and KAS methods have good fitting results for the reduction of Fe_2O_3 by IL at different conversion rates. At the same time, Tables 4 and 5 show that the FWO method has a better linear correlation when calculating activation energy than the KAS method. Therefore, the FWO method is used for discussion here. The relationship between activation energy and conversion rate during the reduction of Fe_2O_3 by IL is also shown in Figure 8. The variation range of reaction activation energy is 241.91~463.51 kJ·mol^{-1}. Overall, the activation energy shows a trend of initially decreasing, then increasing, and finally decreasing slightly as the conversion rate increases.

Table 4. Calculation of kinetic parameters under different conversion rates by FWO method.

Samples	α	Fitting Equation	Activation Energy (E) (kJ·mol^{-1})	Correlation Coefficient (R^2)
IL + Fe_2O_3	0.1	$y = -34{,}342.13x + 37.55$	271.41	1.0000
	0.2	$y = -30{,}609.25x + 32.64$	241.91	0.9720
	0.3	$y = -32{,}761.33x + 33.63$	258.91	0.9867
	0.4	$y = -42{,}029.09x + 41.48$	332.16	0.9917
	0.5	$y = -55{,}936.50x + 53.36$	442.07	0.9971
	0.6	$y = -58{,}503.06x + 54.97$	462.35	0.9982
	0.7	$y = -57{,}055.05x + 53.17$	450.91	0.9995
	0.8	$y = -58{,}030.18x + 53.69$	458.61	0.9951
	0.9	$y = -58{,}649.94x + 53.96$	463.51	0.9951
	0.95	$y = -56{,}633.91x + 52.02$	447.58	0.9975

Table 5. Calculation of kinetic parameters under different conversion rates by KAS method.

	α	Fitting Equation	Activation Energy (E) (kJ·mol^{-1})	Correlation Coefficient (R^2)
IL + Fe_2O_3	0.1	$y = -32{,}402.11x + 21.79$	269.39	0.9999
	0.2	$y = -28{,}606.14x + 16.82$	237.83	0.9681
	0.3	$y = -30{,}683.25x + 17.73$	255.10	0.9850
	0.4	$y = -39{,}894.48x + 25.54$	331.68	0.9909
	0.5	$y = -53{,}753.34x + 37.37$	446.91	0.9968
	0.6	$y = -56{,}287.43x + 38.95$	467.97	0.9980
	0.7	$y = -54{,}818.58x + 37.13$	455.76	0.9994
	0.8	$y = -55{,}777.41x + 37.64$	463.73	0.9947
	0.9	$y = -56{,}385.17x + 37.90$	468.79	0.9947
	0.95	$y = -54{,}362.31x + 35.95$	451.97	0.9973

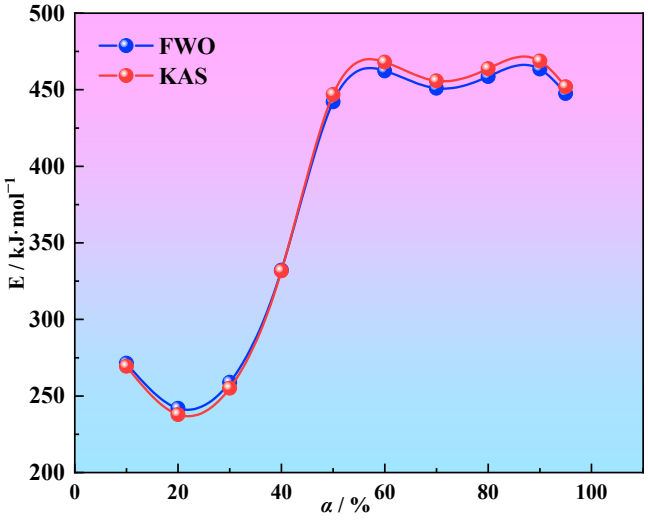

Figure 8. The activation energy change of Fe_2O_3 reduction by IL obtained by FWO and KAS method.

The process of reducing iron oxide by biomass or pulverized coal is a multi-component and multi-phase complex system in which gas/solid phases participate in the reduction reaction. The differential atmosphere conditions caused by the volatiles in the reducing agent will change the thermodynamic and kinetic characteristics of the reduction reaction [48–50]. This is also consistent with the fact that the activation energy of the reduction process of Fe_2O_3 by IL is not a fixed value, indicating that the activation energy and reaction mechanism are different in different temperature ranges. When the temperature is lower than 750 °C, precipitated products mainly include H_2O, CO_2, CO, and CH_4 [51,52]. The

precipitation temperature of free water is mainly concentrated in 80~110 °C, the gas product CH_4 is concentrated in 300~600 °C, CO_2 and CO start at 320 °C, and the yield reaches the maximum at 750 °C. Therefore, the high CO concentration at the beginning of the reaction makes the reduction reaction of Fe_2O_3 easier, and the reaction activation energy also decreases. As the reaction progresses, the reducing agents containing C and H generated by the early pyrolysis of IL will be gradually consumed by the reduction reaction with Fe_2O_3, resulting in the deterioration of the reaction kinetic conditions and the increase of the activation energy. As the reaction temperature continues to rise, the pyrolysis process gradually deepens, which makes the benzene ring in IL break and the char yield increase. At this time, good thermodynamic and kinetic conditions reduce the activation energy.

According to the analysis in Section 3.2, the phase change of Fe_2O_3 reduced by IL is $Fe_2O_3 \rightarrow Fe_3O_4$, $Fe_3O_4 \rightarrow FeO$, $FeO \rightarrow Fe$. Wei et al. [53] believed that the process of carbon reduction of Fe_2O_3 was a step-by-step reduction, and the activation energies of $Fe_3O_4 \rightarrow FeO$ and $FeO \rightarrow Fe$ processes were 628 kJ·mol^{-1} and 648 kJ·mol^{-1}, respectively, while the activation energy of IL reduction of Fe_2O_3 was only 463.51 kJ·mol^{-1}. This is related to the catalytic effect of iron ion on lignin pyrolysis. For example, the research results of Yang et al. [54] show that the presence of Fe_2O_3 has a catalytic effect on the pyrolysis of lignin at 500~800 °C. Wang et al. [55] studied the cracking of biomass tar with dolomite from different producing areas and found that the higher the content of Fe_2O_3 in dolomite, the stronger the cracking ability of tar. The FeS catalyst has an obvious effect on ether bond cleavage of lignin [56]. The above analysis results show that there is a coupling effect in the reduction of Fe_2O_3 by IL, that is, the presence of iron ions catalyzes the pyrolysis reaction of IL, and the pyrolysis products of IL promote the reduction of Fe_2O_3.

4. Conclusions and Prospect

IL is a by-product in the papermaking and pulping industry, which is abundant and underutilized. By studying the mechanism of IL reducing iron oxide, we aim to explore the potential of converting this waste resource into a valuable reducing agent. The results are as follows:

(1) The reduction of Fe_2O_3 by industrial lignin is easier than that by pulverized coal. The mixed sample of industrial lignin and Fe_2O_3 completed the transformation of $Fe_2O_3 \rightarrow Fe_3O_4 \rightarrow FeO \rightarrow Fe$ at 900 °C, while the mixed sample of pulverized coal and Fe_2O_3 completed the transformation at 1100 °C.

(2) Too high a heating rate has an adverse effect on the reduction of Fe_2O_3. On the basis of ensuring both sufficient reduction and reduction efficiency, the optimal heating rate is 10 °C·min^{-1}.

(3) The activation energy of IL reducing Fe_2O_3 varied from 241.91 to 463.51, which was much lower than that of carbon reducing Fe_2O_3. At the reduction fraction $\alpha \leq 0.6$, the activation energy increased rapidly from approx. 271 kJ·mol^{-1} to 462 kJ·mol^{-1}, while it gradually dropped to 447 kJ·mol^{-1} at $\alpha = 0.95$.

(4) Industrial lignin as a reductant has certain advantages in reducing iron oxide compared with pulverized coal, which provides a theoretical basis for the application of other biomass in the field of iron making. However, it is also noted that the sulfur content in industrial lignin is high, and sulfur is a harmful element for iron-making, so how to remove sulfur from industrial lignin is one of the directions that should be studied in the future.

Author Contributions: Conceptualization, D.X. and G.W.; methodology, D.X. and Q.Z. (Qiang Zhang); software, D.X. and Y.W.; validation, D.L. and Q.Z. (Qinghua Zhang); formal analysis, G.W. and H.H.; investigation, D.X. and Q.Z. (Qiang Zhang); resources, G.W.; data curation, D.L.; writing—original draft preparation, D.X. and Y.W.; writing—review and editing, Q.Z. (Qiang Zhang) and D.L.; visualization, H.H. and D.L.; supervision, G.W. and Y.W.; project administration, D.X and Q.Z. (Qinghua Zhang); funding acquisition, Q.Z (Qiang Zhang). All authors have read and agreed to the published version of the manuscript.

Funding: This study was financially supported by the National Natural Science Foundation of China (No. 52105353) and the Linyi University Students' Innovation and Entrepreneurship Project (No. X202410452586).

Data Availability Statement: The original contributions presented in the study are included in the article, further inquiries can be directed to the corresponding author.

Conflicts of Interest: The authors declare no conflicts of interest.

References

1. Zhu, D.C.; Zhu, B.; Geng, A.L.; Li, Y.X.; Xu, L.X. Research progress in lignin-based 3D printing materials. *Appl. Chem. Ind.* **2023**, *52*, 820–826. [CrossRef]
2. Li, M.F.; Xu, Y.H. Fractionation of industrial lignin: A review. *J. For. Eng.* **2023**, *8*, 13–20. [CrossRef]
3. Wang, T.Y.; Li, H.Y.; Diao, X.Y.; Lu, X.B.; Ma, D.G.; Ji, N. Lignin to dispersants, adsorbents, flocculants and adhesives: A critical review on industrial applications of lignin. *Ind. Crops Prod.* **2023**, *199*, 116715. [CrossRef]
4. Nguyen, L.T.; Phan, D.P.; Sarwar, A.; Tran, M.H.; Lee, O.K.; Lee, E.Y. Valorization of industrial lignin to value-added chemicals by chemical depolymerization and biological conversion. *Ind. Crops Prod.* **2021**, *161*, 113219. [CrossRef]
5. Chen, X.Y.; Yuan, B.; Yu, F.L.; Xie, C.X.; Yu, S.T. Lignin: A Potential Source of Biomass-Based Catalysts. *Prog. Chem.* **2021**, *33*, 303–317. [CrossRef]
6. Romhányi, V.; Kun, D.; Pukánszky, B. Correlations among Miscibility, Structure, and Properties in Thermoplastic Polymer/Lignin Blends. *ACS Sustain. Chem. Eng.* **2018**, *6*, 14323. [CrossRef]
7. Luo, S.P.; Cao, J.Z.; McDonald, A.G. Esterification of industrial lignin and its effect on the resulting poly(3-hydroxybutyrate-*co*-3-hydroxyvalerate) or polypropylene blends. *Ind. Crops Prod.* **2017**, *97*, 281–291. [CrossRef]
8. Morandim-Giannetti, A.A.; Agnelli, J.A.M.; Lanças, B.Z.; Magnabosco, R.; Casarin, S.A.; Bettini, S.H.P. Lignin as additive in polypropylene/coir composites: Thermal, mechanical and morphological properties. *Carbohydr. Polym.* **2012**, *87*, 2563–2568. [CrossRef]
9. Frangville, C.; Rutkevičius, M.; Richter, A.; Velev, O.; Stoyanov, S.; Paunov, V. Fabrication of Environmentally Biodegradable Lignin Nanoparticles. *ChemPhysChem* **2012**, *13*, 4235–4243. [CrossRef] [PubMed]
10. Mahmood, N.; Yuan, Z.; Schmidt, J.; Xu, C. Preparation of bio-based rigid polyurethane foam using hydrolytically depolymerized Kraft lignin via direct replacement or oxypropylation. *Eur. Polym. J.* **2015**, *68*, 1–9. [CrossRef]
11. Silva, E.A.B.d.; Zabkova, M.; Araújo, J.D.; Cateto, C.A.; Barreiro, M.F.; Belgacem, M.N.; Rodrigues, A.E. An integrated process to produce vanillin and lignin-based polyurethanes from Kraft lignin. *Chem. Eng. Res. Des.* **2009**, *87*, 1276–1292. [CrossRef]
12. Yadav, V.K.; Gupta, N.; Kumar, P.; Dashti, M.G.; Tirth, V.; Khan, S.H.; Yadav, K.K.; Islam, S.; Choudhary, N.; Algahtani, A.; et al. Recent Advances in Synthesis and Degradation of Lignin and Lignin Nanoparticles and Their Emerging Applications in Nanotechnology. *Materials* **2022**, *15*, 953. [CrossRef]
13. Liu, H.; Cheng, L.-Q.; Zhou, J.-H. Recent Advances in Low-Cost Carbon Fiber Manufacture from Lignin. *Heilongjiang Pulp Pap.* **2018**, *46*, 18–22.
14. Kun, D.; Pukánszky, B. Polymer/lignin blends: Interactions, properties, applications. *Eur. Polym. J.* **2017**, *93*, 618–641. [CrossRef]
15. Supanchaiyamat, N.; Jetsrisuparb, K.; Knijnenburg, J.T.N.; Tsang, D.C.W.; Hunt, A.J. Lignin materials for adsorption: Current trend, perspectives and opportunities. *Bioresour. Technol.* **2019**, *272*, 570–581. [CrossRef] [PubMed]
16. Liu, J.P. Study on Efficient Depolymerization of Lignin in Hydrogen Donor Solvents for the Preparation of Phenolic Chemicals. Ph.D. Thesis, Beijing University of Chemical Technology, Beijing, China, 2023. [CrossRef]
17. Kawamoto, H. Lignin pyrolysis reactions. *J. Wood Sci.* **2017**, *63*, 117–132. [CrossRef]
18. Asmadi, M.; Kawamoto, H.; Saka, S. Gas- and solid/liquid-phase reactions during pyrolysis of softwood and hardwood lignins. *J. Anal. Appl. Pyrolysis.* **2011**, *92*, 417–425. [CrossRef]
19. Hosoya, T.; Kawamoto, H.; Saka, S. Role of methoxyl group in char formation from lignin-related compounds. *J. Anal. Appl. Pyrolysis.* **2009**, *84*, 79–83. [CrossRef]
20. Liu, W.J.; Jiang, H.; Yu, H.Q. Thermochemical Conversion of Lignin to Functional Materials: A Review and Future Directions. *Green Chem.* **2015**, *17*, 4888–4907. [CrossRef]
21. Meier, D.; Ante, R.; Faix, O. Catalytic hydropyrolysis of lignin: Influence of reaction conditions on the formation and composition of liquid products. *Bioresour. Technol.* **1992**, *40*, 171–177. [CrossRef]
22. Mullen, C.A.; Boateng, A.A. Catalytic pyrolysis-GC/MS of lignin from several sources. *Fuel Process. Technol.* **2010**, *91*, 1446–1458. [CrossRef]
23. Santana, J.A.; Carvalho, W.S.; Ataíde, C.H. Catalytic effect of ZSM-5 zeolite and HY-340 niobic acid on the pyrolysis of industrial kraft lignins. *Ind. Crops Prod.* **2018**, *111*, 126–132. [CrossRef]
24. Figueiredo, P.; Lintinen, K.; Hirvonen, J.T.; Kostiainen, M.A.; Santos, H.A. Properties and chemical modifications of lignin: Towards lignin-based nanomaterials for biomedical applications. *Prog. Mater. Sci.* **2018**, *93*, 233–269. [CrossRef]
25. Pan, K.; Tian, M.; Jiang, Z.-H.; Kjartanson, B.; Chen, A. Electrochemical oxidation of lignin at lead dioxide nanoparticles photoelectrodeposited on TiO_2 nanotube arrays. *Electrochim. Acta* **2012**, *60*, 147–153. [CrossRef]
26. Li, S.H.; Liu, S.; Colmenares, J.C.; Xu, Y.J. A sustainable approach for lignin valorization by heterogeneous photocatalysis. *Green Chem.* **2016**, *18*, 594–607. [CrossRef]

27. Chatel, G.; Rogers, R. Review: Oxidation of Lignin Using Ionic Liquids—An Innovative Strategy To Produce Renewable Chemicals. *ACS Sustain. Chem. Eng.* **2014**, *2*, 322–339. [CrossRef]
28. Schutyser, W.; Renders, T.; Van den Bosch, S.; Koelewijn, S.-F.; Beckham, G.; Sels, B. Chemicals from lignin: An interplay of lignocellulose fractionation, depolymerisation, and upgrading. *Chem. Soc. Rev.* **2018**, *47*, 852–908. [CrossRef] [PubMed]
29. Zaheer, M.; Kempe, R. Catalytic Hydrogenolysis of Aryl Ethers: A Key Step in Lignin Valorization to Valuable Chemicals. *ACS Catal* **2015**, *5*, 1675–1684. [CrossRef]
30. Galkin, M.V.; Sawadjoon, S.; Rohde, V.; Dawange, M.; Samec, J.S.M. Mild Heterogeneous Palladium-Catalyzed Cleavage of β-O-4′-Ether Linkages of Lignin Model Compounds and Native Lignin in Air. *ChemCatChem* **2014**, *6*, 179–184. [CrossRef]
31. Lu, J.; Wang, M.; Zhang, X.; Heyden, A.; Wang, F. β-O-4 Bond Cleavage Mechanism for Lignin Model Compounds over Pd Catalysts Identified by Combination of First-Principles Calculations and Experiments. *ACS Catal* **2016**, *6*, 5589–5598. [CrossRef]
32. Zhou, M.; Fakayode, O.A.; Ahmed Yagoub, A.E.; Ji, Q.; Zhou, C. Lignin fractionation from lignocellulosic biomass using deep eutectic solvents and its valorization. *Renew. Sustain. Energy Rev.* **2022**, *156*, 111986. [CrossRef]
33. Wang, J.H.; Cao, F.; Su, E.; Zhao, L.; Qin, W. Improvement of Animal Feed Additives of Ginkgo Leaves through Solid-state Fermentation using Aspergillus niger. *Int. J. Biol. Sci.* **2018**, *14*, 736–747. [CrossRef] [PubMed]
34. Wang, J.H.; Cao, F.; Su, E.; Wu, C.; Zhao, L.; Ying, R. Improving Flavonoid Extraction from Ginkgo biloba Leaves by Prefermentation Processing. *J. Agric. Food Chem.* **2013**, *61*, 5783–5791. [CrossRef]
35. Liu, Q.M. Preparation of Lignin-Based Carbon Supported Metal Catalysts and Their Reductive Depolymerization of Lignin. Master's Thesis, Tianjin University of Science and Technology, Tianjin, China, 2022. [CrossRef]
36. Wang, Y.P. Stydies on Lignin Depolymerization and Its Structure. Ph.D. Thesis, Beijing University of Chemical Technology, Beijing, China, 2021. [CrossRef]
37. Xiang, D.W.; Shen, F.M.; Jiang, X.; An, H.W.; Zheng, H.Y.; Gao, Q.J. Pyrolysis Characteristics of Industrial Lignin for Use as a Reductant and an Energy Source for Future Iron Making. *ACS Omega* **2021**, *6*, 3578–3586. [CrossRef] [PubMed]
38. Zhang, S. Design and Practice of Grate Rotary Kiln Annular Cooler Oxidation Pellet Process. *Shanxi Met.* **2022**, *45*, 91–93. [CrossRef]
39. Luo, G.P.; Zhang, G.C.; Liu, J.T.; Shang, C.J.; Wang, M.F.; Wu, S.L. Process Optimization for Improving Crushing Strength of Preheated Pellets in Grate-Kiln Oxidied Pelletizing Process. *J. Iron Steel Res.* **2013**, *25*, 13–16+22. [CrossRef]
40. Huang, F.R.; Wang, X.Q.; Li, S.J. The thermal stability of polyetherimide. *Polym. Degrad. Stab.* **1987**, *18*, 247–259. [CrossRef]
41. Liang, Y.G.; Cheng, B.; Si, Y.B.; Cao, D.J.; Jiang, H.Y.; Han, G.M.; Liu, X.H. Thermal decomposition kinetics and characteristics of Spartina alterniflora via thermogravimetric analysis. *Renew. Energy* **2014**, *68*, 111–117. [CrossRef]
42. Sava, I.; Ada, B.; Lisa, G. Study of thermal behavior of polyimides containing pendent-substituted azobenzene units. *Polym. Bull.* **2014**, *71*, 1359–1373. [CrossRef]
43. Pitchaimari, G.; Vijayakumar, C.T. Functionalized N-(4-Hydroxy phenyl) Maleimide Monomers: Kinetics of Thermal Polymerization and Degradation Using Model-Free Approach. *J. Appl. Polym. Sci.* **2014**, *131*, 2896308. [CrossRef]
44. Starink, M.J. The determination of activation energy from linear heating rate experiments: A comparison of the accuracy of isoconversion methods. *Thermochim. Acta* **2003**, *404*, 163–176. [CrossRef]
45. Hao, S.J.; Sun, T.H.; Jiang, W.F.; Zhang, Y.Z.; Lan, J.R. Reduction Behavior of Bituminous Coal Coated Magnetite Powder. *Iron Steel Vanadium Titan.* **2019**, *40*, 102–106.
46. Zhong, S.P.; Guo, L.; Ding, Z.Y.; Guo, Z.C. observation on the growth of iron whiskers in the process of direct reduction of iron ore powder by gas. Nonferrous Met. *Sci. Eng.* **2018**, *9*, 15–21. [CrossRef]
47. Ren, N.; Wang, F.; Zhang, J.J.; Zheng, X.F. Progress in Thermal Analysis Kinetics. *Acta Phys.-Chim. Sin.* **2020**, *36*, 1905062. [CrossRef]
48. Pineau, A.; Kanari, N.; Gaballah, I. Kinetics of reduction of iron oxides by H_2: Part II. Low temperature reduction of magnetite. *Thermochim. Acta* **2007**, *456*, 75–88. [CrossRef]
49. Pineau, A.; Kanari, N.; Gaballah, I. Kinetics of reduction of iron oxides by H_2: Part I: Low temperature reduction of hematite. *Thermochim. Acta* **2006**, *447*, 89–100. [CrossRef]
50. Mi, Q.Y. Kinetic Mechanism of Direct Reduction of Iron Ore Reinforced by High Volatile Coal. Master's Thesis, Xi'an University of Architecture and Technology, Xi'an, China, 2023. [CrossRef]
51. Zhang, X.Z.; Liu, T.Q.; Zhang, W.L.; Guo, D.L.; Wang, L.F.; Chen, M.W. Effect of pyrolysis conditions on pyrolysis and gasification characteristics of black liquor. *China Pulp Pap. Ind.* **2016**, *37*, 77–81. [CrossRef]
52. Guo, D.L.; Wu, S.B.; Liu, B.; Yin, X.L.; Yang, Q. Catalytic effects of NaOH and Na_2CO_3 additives on alkali lignin pyrolysis and gasification. *Appl. Energy* **2012**, *95*, 22–30. [CrossRef]
53. Wei, R.F.; Cang, D.Q.; Zhang, L.L.; Bai, Y.Y. Staged reaction kinetics and characteristics of iron oxide direct reduction by carbon. *Int. J. Miner. Metall. Mater.* **2015**, *22*, 1025–1032. [CrossRef]
54. Wang, H.P. The Experiment and Mechism Study on Palm Oil Wastes Pyrolysis. Ph.D. Thesis, Huazhong University of Science and Technology, Wuhan, China, 2005. [CrossRef]
55. Wang, T.J.; Chang, J.; Lv, P.M. Novel Catalyst for Cracking of Biomass Tar. *Energy Fuels* **2005**, *19*, 22. [CrossRef]
56. Sui, X.J.; Wu, S.B. Preparation of phenols using thermal chemical conversion of industrial kraft lignin. *CIESC J.* **2011**, *62*, 1763–1769. [CrossRef]